Sendai virus recruits cellular villin to remodel actin cytoskeleton during fusion with hepatocytes

Sunandini Chandra[a], Raju Kalaivani[b,c], Manoj Kumar[a], Narayanaswamy Srinivasan[b], and Debi P. Sarkar[a,d,*]

[a]Department of Biochemistry, University of Delhi, New Delhi 110021, India; [b]Molecular Biophysics Unit, Indian Institute of Science, Bengaluru 560012, India; [c]MRC Laboratory of Molecular Biology, Cambridge CB20QH, UK; [d]Indian Institute of Science Education and Research, Mohali, Manauli PO 140306, Punjab, India

ABSTRACT Reconstituted Sendai viral envelopes (virosomes) are well recognized for their promising potential in membrane fusion–mediated delivery of bioactive molecules to liver cells. Despite the known function of viral envelope glycoproteins in catalyzing fusion with cellular membrane, the role of host cell proteins remains elusive. Here, we used two-dimensional differential in-gel electrophoresis to analyze hepatic cells in early response to virosome-induced membrane fusion. Quantitative mass spectrometry together with biochemical analysis revealed that villin, an actin-modifying protein, is differentially up-regulated and phosphorylated at threonine 206—an early molecular event during membrane fusion. We found that villin influences actin dynamics and that this influence, in turn, promotes membrane mixing through active participation of Sendai viral envelope glycoproteins. Modulation of villin in host cells also resulted in a discernible effect on the entry and egress of progeny Sendai virus. Taken together, these results suggest a novel mechanism of regulated viral entry in animal cells mediated by host factor villin.

INTRODUCTION

Sendai virus (SeV), a prototype of the *Paramyxoviridae* family, binds to the host cell surface through its hemagglutinin-neuraminidase glycoprotein (HN). This binding also triggers the fusion protein (F), another envelope glycoprotein to undergo a conformational change and catalyze the mixing of viral and cellular lipid membranes (Okada, 1988). Productive SeV infection depends on these two initial steps of membrane fusion–mediated viral entry. Virosomes bearing these glycoproteins (HNFV) can be exploited to deliver biomolecules to mammalian cells, both in vitro and in vivo (Blumenthal and Loyter, 1991; Kim *et al.*, 2008). In a preclinical study, we demonstrated that Sendai F-virosomes (FV, devoid of HN) can be used for targeted delivery of drugs and therapeutic genes in hepatocytes, both in culture and whole animal (Ramani *et al.*, 1998; Wang *et al.*, 2009). However, a significant reduction of fusion activity due to the absence of HN in such FV-mediated delivery warrants investigation of compensatory cellular factors in the regulation of membrane fusion.

Recent studies with enveloped viruses indicate an active involvement of host machinery for an efficient entry process (Pleschka *et al.*, 2001; Greber, 2002; Harmon and Ratner, 2008; Luthra *et al.*, 2008),

although the key aspects of the cellular regulatory mechanism of membrane fusion, per se, remain to be fully understood. With a view to address this concern, we investigated whether, in addition to cell surface receptor(s) for HN–mediated attachment (Verma, Mani, Sharma, et al., 2005; Krishnan, Verma, et al., 2009), SeV requires other host factors for efficient fusion. We have demonstrated earlier that the extracellular signal-regulated kinases (ERKs) promote viral fusion via actin cytoskeletal rearrangements, while AKT1 attenuates this process (Sharma et al., 2010). The present investigation was undertaken to identify host effector molecule(s) modulating this regulation in conjunction with cytoskeletal elements during viral entry. The importance of actin cytoskeleton and its reorganization in affecting the overall viral life cycle of enveloped fusogenic viruses, starting from entry to egress, is well documented (Taylor, Koyuncu, and Enquist, 2011). We performed a systematic high-resolution global examination of proteome alterations occurring solely because of membrane fusion. Our analysis revealed that certain host cell proteins are differentially regulated during HNFV–cell fusion. Of these, we focused on villin, a unique actin-binding protein (ABP) that nucleates, caps, bundles, and severs actin filaments (Khurana, 2006; Khurana and George, 2008). The role of villin as an actin modulator in the regulation of cell structure, function, and plasticity has been extensively studied (Khurana, 2006; Khurana and George, 2008; George et al., 2013). Villin is also implicated in pathogenic Gram-negative bacterial invasion of intestinal epithelial cells (Athman et al., 2005; Lhocine et al., 2015). However, its role in the entry process of fusogenic enveloped viruses is yet unexplored.

To address the possibility of villin contributing to the efficacy of virosome–liver cell fusion, we then investigated the effect of villin in HNFV-HepG2 cell fusion. Knockdown of endogenous villin in HepG2 cells resulted in a drastic reduction in membrane fusion. A detailed analysis of actin dynamics led us to decipher a molecular mechanism involving villin–actin interaction to regulate virosome–cell fusion. Additionally, modulation of villin caused a concomitant effect on SeV infection of host cells. Altogether, these data support a previously unidentified function of villin as a host cell cofactor in specific regulation of membrane fusion. Thus, our study provides, for the first time, an insight into the role of villin in modulating the actin cytoskeleton during the early event of membrane fusion mediated by viral glycoproteins.

RESULTS

Villin is differentially regulated during membrane fusion of Sendai virosomes with HepG2 cells

To detect a comprehensive change in the proteome of the target cells during membrane fusion, we performed highly sensitive two-dimensional (2D) difference gel electrophoresis (DIGE) analysis of total cell lysates of HepG2 cells fused with HNFV. In combination with mass spectrometry, this technique can detect minute changes in protein expression in a cell or tissue system under specific experimental conditions (Corte et al., 2008; Huang et al., 2009; Kondo and Hirosashi, 2009; Vester et al., 2009; Jin et al., 2010; Muroi et al., 2010; Xiao, Wang, et al., 2010). Total protein extract of HepG2 cells fused with HNFV for 30 or 60 min were subjected to the analysis. Lysate from cells incubated with heat-inactivated HNFV (HNFVHC [HNFV heat control], fusogenically inactive but capable of binding to the cell surface) was used as a negative control. Throughout our study, in both control and experimental conditions, cells were treated with 10 mM sodium azide to block endocytosis, thus allowing information to be extracted solely because of membrane fusion (Bagai and Sarkar, 1994). The 2D-DIGE analysis revealed several protein spots that were differentially regulated upon membrane

fusion. Protein spots of interest were selected based on statistical significance ($p \leq 0.02$), clustering between the gels, and having at least 1.2-fold change against the control (Figure 1, A and B). Tandem mass spectrometry (MS/MS; Orbitrap) along with the SEQUEST data analysis program identified eight differentially regulated proteins. Among those, villin was maximally up-regulated (~1.34-fold; Table 1). This increment was seen at the 1 h time point but is undetected at 30 min of fusion (Figure 1, C–E). Actin cytoskeleton regulatory proteins such as alpha-actinin 4 and actin-related protein 3 (Arp3) were also up-regulated, although to a lesser extent. Down-regulation of annexin A4, which is implicated in related events such as endocytosis/exocytosis (Gerke and Moss, 2002), was also observed. Proteins such as peptidyl-prolyl cis-trans isomerase FKBP4 and protein DJ-1 were down-regulated, presumably because of cellular stress induced by membrane fusion (Shendelman et al., 2004; Gallo et al., 2011; Eltoweissy et al., 2016). Rho GDP-dissociation inhibitor 1, a regulator of Rho GTPases involved in actin cytoskeleton rearrangement (Sun and Barbieri, 2004), was also down-regulated. Other proteins such as X-ray repair cross-complementing protein 5 were also modulated during fusion, but the relevance of this finding is yet to be ascertained. Among all the known ABPs, villin is an abundant epithelial actin-modifying protein responsible for fine regulation of actin dynamics in cells, including capping, severing, nucleating, and bundling actin filaments (Khurana and George, 2008). Moreover, studies have reported the involvement of actin cytoskeletal remodeling in fusion-mediated entry of enveloped viruses (Taylor, Koyuncu, and Enquist, 2011). Also, numerous reports have suggested that villin exhibits a seminal role in actin dynamics in response to many patho-physiological stresses (Khurana, 2000; Athman et al., 2003, 2005; Khurana and George, 2008; Lhocine et al., 2015). As we reported earlier, virus-induced host cell membrane fusion in liver cells may also be regarded as a trigger for stress response (Sharma et al., 2010). Hence, we prioritized villin in this study.

The proteomic data were then validated through 2D immunoblotting. As shown in Figure 1, F (top row) and G, a substantial increase (~70% higher than HNFVHC) in villin expression was observed in cells fused with HNFV. Moreover, an extra spot recognized by the villin antibody was observed in fusion samples, which suggested a posttranslational modification (Figure 1F, top row, green arrow). The possibilities of glycosylation and sulfation were less likely, as examined by the Sulfinator tool (ExPASy) and supported by published literature (Bretscher and Weber, 1980). Further, an increase in villin was associated with an increase in the intensity of phosphorylated ERK levels in the fusion samples. The intensity of phosphorylated forms (toward the acidic end of the gel) was higher, and an extra spot in leftmost position corresponding to ERK was also observed in case of fusion (Figure 1F, middle row, red arrow). This is in agreement with our earlier report demonstrating the activation of mitogen-activated protein kinase (MAPK) during membrane fusion (Sharma et al., 2010). However, the increase in villin protein level was not accompanied by an increment in the transcript levels (Figure 1J). To account for the enhancement of villin during fusion, 2D immunoblot analysis was performed where fusion was carried out in the presence of cycloheximide (a commonly used translational inhibitor) for 1 h. As shown in Figure 1H, top row, a sustained high level of villin was seen in cells fused with HNFV (~2.85-fold higher in fusion; Figure 1I). Even in the absence of active translation, an extra spot toward the acidic end was observed, indicating a possible posttranslational modification. Reprobing the same blot confirmed the phosphorylation of villin at threonine residue (Figure 1H, middle row, blue arrow). Taken together, our results
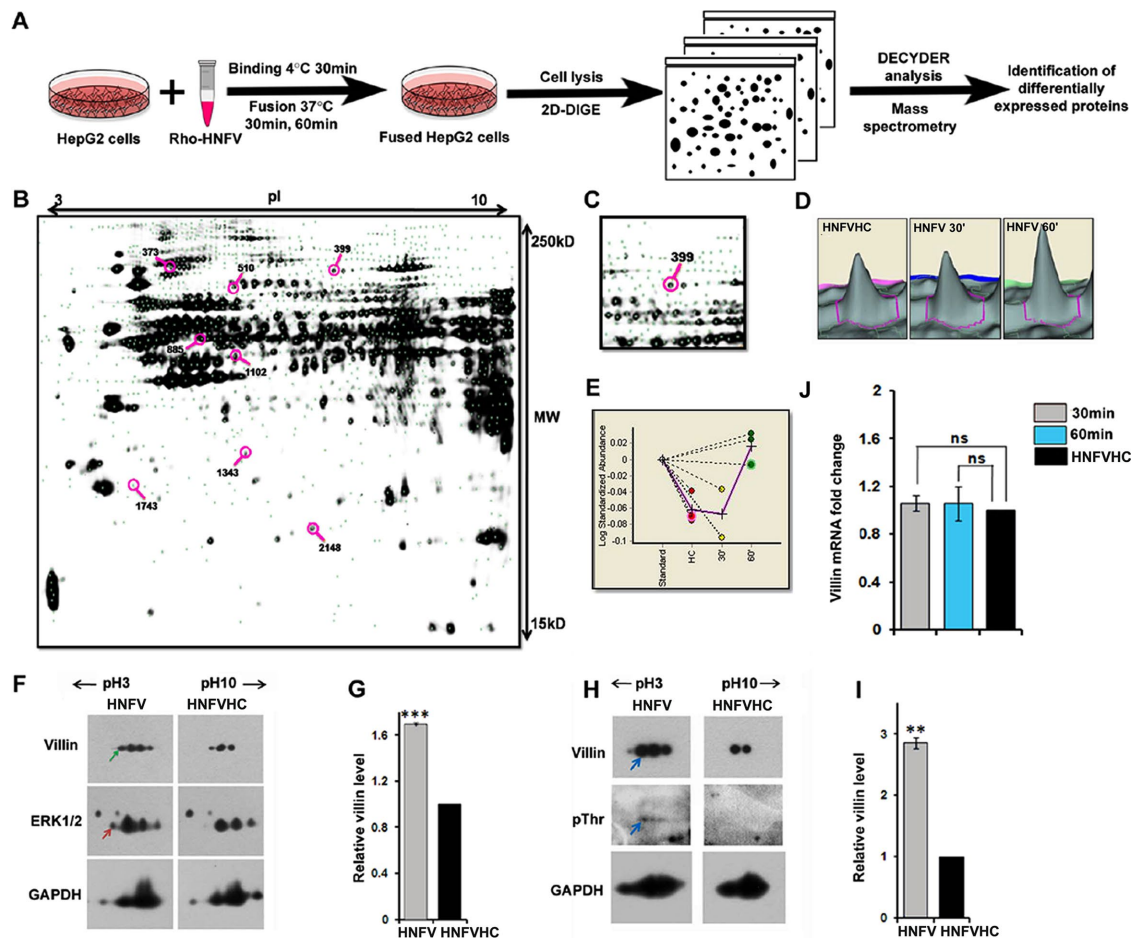
FIGURE 1: Protein spots differentially regulated during membrane fusion and villin profile in HepG2 cell extracts during membrane fusion visualized by 2D immunoblot. (A) Schematic overview of the workflow. (B) Representative 2D-DIGE gel image of HepG2 cell proteome upon fusion with virosomes (HNFV). The positions of eight differentially abundant protein spots selected for protein identification are indicated. Their molecular identities are indicated in Table 1. (C) Spot 399 identified to be villin and (D) 3D view of spot 399 in HNFVHC, 30 min, and 60 min samples. Time of fusion of HNFV with HepG2 cells is indicated by 30′ and 60′. HNFVHC indicates negative control where HNFV was heat inactivated. (E) Graphical view of standardized abundance value of spot 399. (F) HepG2 cells were subject to membrane fusion for 60 min and cell extracts (75 μg) were processed for 2D-gel electrophoresis followed by immunoblotting for villin, ERK1/2, and GAPDH (loading control) sequentially. Green arrow and red arrow indicate additional spot of villin and ERK, respectively, in fused cells. (G) Relative fold change in villin levels during membrane fusion, expressed as mean ± SEM, $n = 5$. (H) HepG2 cells were subject to membrane fusion in the presence of cycloheximide. Cell extracts (150 μg) were processed for 2D-gel electrophoresis followed by immunoblotting for villin, phosphothreonine, and GAPDH sequentially. Blue arrows indicate villin phosphorylation. (I) Relative fold change of villin expressed as mean ± SEM, $n = 5$. (J) Villin mRNA fold change in fusion samples versus negative HNFVHC. ***$p < 0.001$; **$p < 0.01$; MW, molecular weight; ns, not significant.

indicate that villin is differentially up-regulated and threonine phosphorylated during virosome–host cell membrane fusion.

Villin promotes virosome–host cell fusion (lipid mixing)

To examine the role of villin in membrane fusion, we used a fluorescent lipid probe (Rhod-PE) dequenching-based technique. This technique of evaluating membrane fusion (Figure 2A) is based on lipid bilayer mixing, the primary step in virosome–cell fusion (Bagai et al., 1993), where the extent of fusion is expressed as the percentage of fluorescence dequenching (FDQ). We knocked down villin in HepG2 cells using specific small interfering RNAs (siRNAs) and found undetectable protein (Figure 2C), significant down-regulation of mRNA (>80%, Figure 2D), and highly reduced villin immunostaining (>95% reduction, Supplemental Figure S1). Loss of villin in HepG2 cells resulted in a 40–50% reduction in lipid

mixing in terms of both rate and extent (Figure 2B). In villin-depleted cells, microscopic monitoring of the increase in fluorescence intensity of Rhod-PE due to dequenching during its diffusion in the host cell lipid bilayer (Figure 2E, bottom vs. top panel) also revealed an ~2-fold reduction in rhodamine fluorescence, suggesting that villin escalates lipid mixing during HNFV-mediated membrane fusion (Figure 2F). Interestingly, villin overexpression in HepG2 cells did not result in any further enhancement of fusion over basal levels as measured by FDQ analysis (Figure 2, G and H). This suggests endogenous villin in HepG2 cells to be present at a threshold level required for fusion.

To assess whether villin affects core mixing (including lipid mixing followed by aqueous pore formation) as well, we studied fusion with HNFV loaded with rhodamine isothiocyanate (RITC)-conjugated lysozyme (aqueous probe for monitoring fusion pore formation) in

Spot ID	Peptides matched (unique)	Accession no. (International Protein Index)	Protein name/ID	Gene symbol	Molecular weight	Isoelectric point	Fold change	Score	Sequence coverage
373	36 (20)	IPI00013808.1	Alpha-actinin-4	ACTN4	104.8	5.44	1.27	455	45.01
399	34 (31)	IPI00218852.4	Villin-1	VIL1	92.64	6.39	1.34	441	53.33
510	23 (23)	IPI00220834.8	X-ray repair cross-complementing protein 5	XRCC5	82.65	5.81	1.23	334	61.34
885	11 (11)	IPI00219005.3	Peptidyl-prolyl cis-trans isomerase FKBP4	FKBP4	51.77	5.43	–1.4	74	35.73
1102	13 (11)	IPI00028091.3	Actin-related protein 3	ARP3	47.34	5.88	1.21	171	37.56
1343	19 (18)	IPI00793199.1	Annexin A4	ANXA4	36.06	6.12	–1.5	1418	50.16
1743	7 (7)	IPI00003815.3	Rho GDP-dissociation inhibitor 1	ARHGDIA	23.19	5.11	–1.43	88	26.47
2148	12 (12)	IPI00298547.3	Protein DJ-1	PARK7	19.88	6.78	–1.27	184	73.54

TABLE 1: Proteins identified by mass spectrometry that were differentially expressed during HNFV–HepG2 fusion.

villin knockdown HepG2 cells. We observed that down-regulation of villin in HepG2 cells led to a ~2-fold decrease in RITC-lysozyme delivery to the cytosol of HepG2 cells (Figure 3, A–C). These results further suggest the role of villin in the fusion process, in terms of both membrane and core mixing. It may be pertinent to mention here that for membrane fusion induced by all wild-type viral fusion glycoproteins (barring its C-terminal–truncated mutants [Kemble et al., 1994; Bagai and Lamb, 1996]), lipid probe–based FDQ assay is complementary to core mixing assay (Sarkar et al., 1989; Krishnan, Verma, et al., 2009; Sharma et al., 2010), and hence the former was used throughout this study.

Villin associates with actin during membrane fusion and undergoes threonine phosphorylation

To further understand the role of villin in membrane fusion, we focused on the possibility of villin–actin interaction during cytoskeletal rearrangements required for fusion. Because filamentous actin (F-actin) migrates to insoluble fractions during cell fractionation, postfusion extracts of HepG2 cells were fractionated into soluble and insoluble portions. The obtained fractions were validated by detection of villin, actin, and glyceraldehyde-3-phosphate dehydrogenase (GAPDH) (marked "INPUT" in Figure 4A, top) and investigated for coimmunoprecipitation of villin using anti-villin antibody and detection by Western blotting (Figure 4A, bottom). This approach confirmed strong physical association of villin with ß-actin (actin, cytoplasmic 1, ACTB) in Triton-insoluble extracts after fusion (~28.7-fold higher; Figure 4C). Although in a lesser amount, actin was also present in Triton-soluble fractions of fusion samples but was completely absent in that of negative control (HNFVHC). This was interesting as the Triton-insoluble fraction of a host cell is known to be rich in F-actin cytoskeleton. Villin was found to be associated with actin in the Triton-insoluble fraction of fused cells (Figure 4A, bottom, bottom row) and was phosphorylated at threonine (~1.52-fold, Figure 4B) in accordance with our previous observation of Ser/Thr MAPK activation during fusion (Sharma et al., 2010). To identify the threonine residue in villin that gets phosphorylated, we used two different approaches: 1) in silico analyses and 2) immunoprecipitation coupled with liquid chromatography–MS/MS (LC-MS/MS).

Our in silico analysis approach, ConSeq (Berezin et al., 2004), identified 11 of the 46 threonine residues in full-length villin as being highly conserved and solvent exposed. The rationale was that the p-threonine site, if crucial for the regulation of membrane fusion, would be conserved during the course of divergent evolution. Eleven such conserved sites (amino acids 83, 183, 206, 328, 503, 523, 528, 634, 684, 693, and 708; see Supplemental Table S1 for details) were found in human villin. Independently, evidence of threonine phosphorylation at amino acids 2, 15, 206, 350, 506, and 693 came from phosphoproteome studies documented in PhosphoSitePlus (Hornbeck et al., 2012). Put together, these data suggest the possibility of phosphorylation at two sites, T206 and T693. To gain experimental evidence of this, we immunoprecipitated villin from extracts of fused cells and performed in-gel digestion of the band corresponding to the molecular weight of villin followed by mass spectrometry. LC-MS/MS and analysis of its spectra showed villin to be phosphorylated at threonine 206 upon membrane fusion with Sendai virosomes (Supplemental Figure S2).

Villin induces actin reorganization to enhance membrane fusion

Upon establishing the interaction of villin with actin during fusion, we tested whether it involves modulation of actin dynamics. We measured globular actin (G-actin) and F-actin content of HepG2 cells at
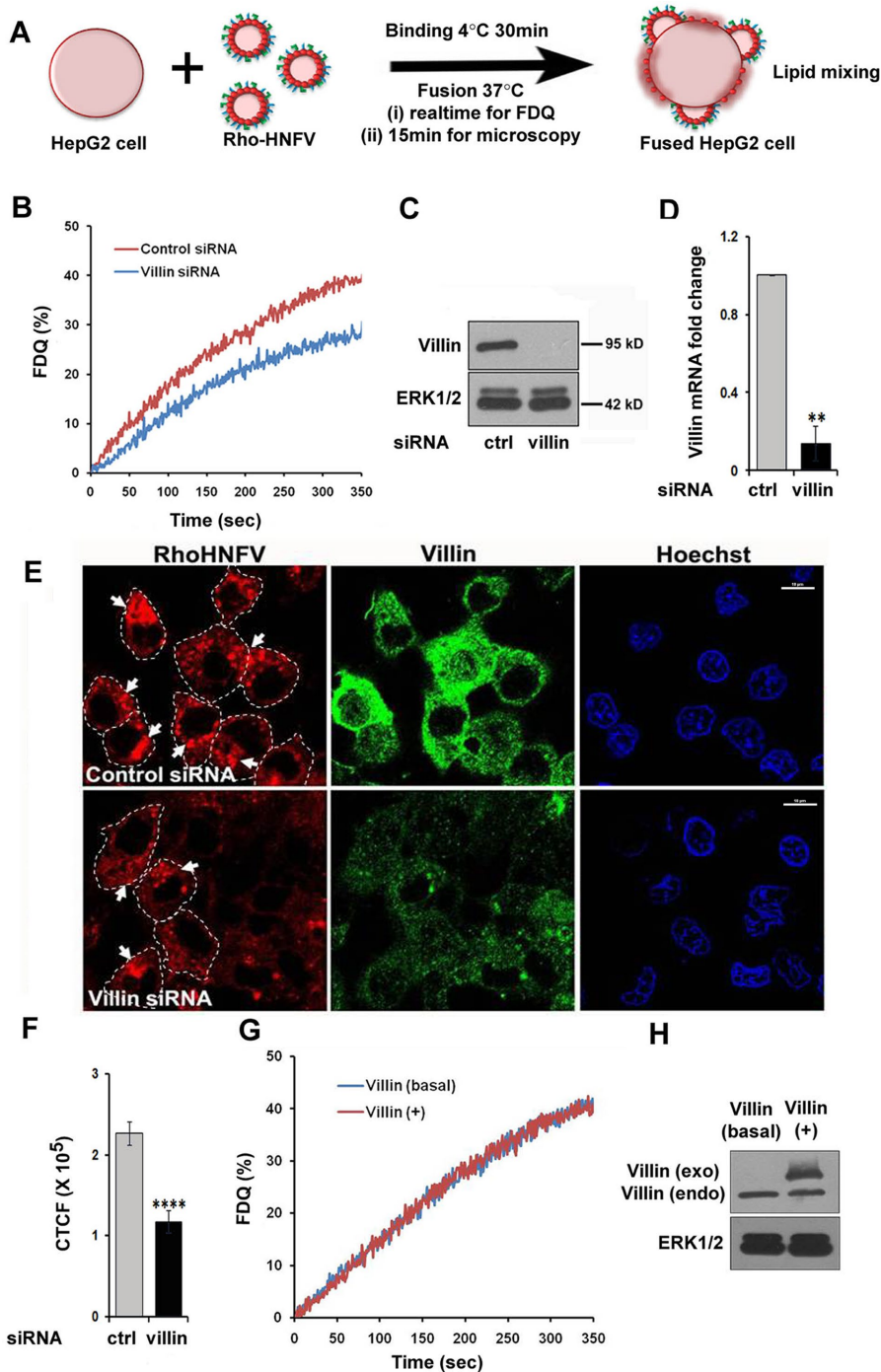
FIGURE 2: Down-regulation of villin reduces fusion of HepG2 cells with virosomes. (A) Schematic overview of workflow to study lipid mixing. (B) Cells transfected with control or villin-specific siRNA were processed 72 h posttransfection and allowed to bind with Rhod-PE–labeled HNFV (RhoHNFV), followed by measurement of fusion kinetics. Extent of fusion was expressed as percentage FDQ. Individual spectrum represents online recorded FDQ of one of the three independent experiments. (C) Western blot and (D) mRNA profile of villin in cells from panel B. (E) HepG2 cells were transfected with control or villin-specific siRNA. Cells were allowed to bind and fuse with RhoHNFV 72 h posttransfection. Cells were fixed, immunostained for villin, counterstained with Hoechst, and processed for confocal microscopy. Arrows denote diffusion of Rhod-PE indicating membrane fusion. Dotted lines denote boundaries of HNFV-fused cells. (F) CTCF expressed as mean ± SEM, $n = 25$. (G) HepG2 cells transfected with plasmid expressing villin were allowed to bind with RhoHNFV, followed by measurement of FDQ. Individual spectrum represents online recorded FDQ of one of the three independent experiments. (H) Immunoblot profile of exogenous and endogenous villin in cells used in G. $**p < 0.01$; $****p < 0.0001$; ctrl, control. Scale bars, 10 µm.

0, 5, 15, 30, and 60 min postfusion with active HNFV or HNFVHC, after binding at 4°C for 40 min. Compared with binding in the case of HNFVHC, the ratio of G/F-actin markedly decreased during the initial 5 min of fusion (~4.5-fold decrease; Figure 5, A, second panel from top, and C, red bars). This decrease was lesser at 15 min of fusion (an approximately twofold decrease; Figure 5, A, third panel from top, and C, gray bars), recovered thereafter at 30 min (~1.3-fold decrease; Figure 5, A, fourth panel from top, and C, light blue bars), and restored to normal at 60 min (Figure 5, A, bottom panel, and C, black bars). The observed effect on the altered ratio of G/F-actin signifying actin dynamics requires active fusion, as binding alone in case of HNFVHC or active HNFV for 0 min fusion did not affect the G/F-actin ratio (Figure 5, A, first panel from top, and C, dark blue bars). It is thus likely that membrane fusion initially induced actin polymerization but that this was followed by depolymerization to eventually bring the ratio back to normal. Interestingly, silencing of villin expression also leads to a slight increase in F-actin with a concomitant decrease in G/F-actin ratio in cells that have undergone fusion for even 5 min when compared with cells treated with HNFVHC (Figure 5, B and C, red bars plotted under "villin knockdown").

To test whether the change in G/F-actin ratio is dependent on virosome fusion, we also performed this analysis in cells (with and without villin) in the absence of virosomes. No significant change in the ratio here indicates that virosome fusion acts as a trigger in concert with villin to induce actin dynamics (Supplemental Figure S3, A and B).

The F-actin content and distribution was also visualized by phalloidin stain (Figure 5D and Supplemental Figure S3) after both 5 and 15 min of fusion. As shown in Figure 5D (first and second rows), actin distribution is altered in cells undergoing fusion. F-actin levels were increased and concentrated in the cell cortex, where it colocalized with villin (Figure 5G, merge of red and green is seen throughout the Z-stack from the side view). Such colocalization was not seen in the absence of fusion when cells were incubated with HNFVHC (Figure 5H). It is relevant to note that the localization of villin also altered during membrane fusion. In fused cells, villin was located mainly at the periphery of the cells (colocalized with actin), whereas in control cells, there was a more diffuse pattern (Figure 5D, compare the first and second rows). Such cortical association of villin and actin could be observed as early as at 5 min of fusion with active virosomes (Supplemental Figure S3C, compare the
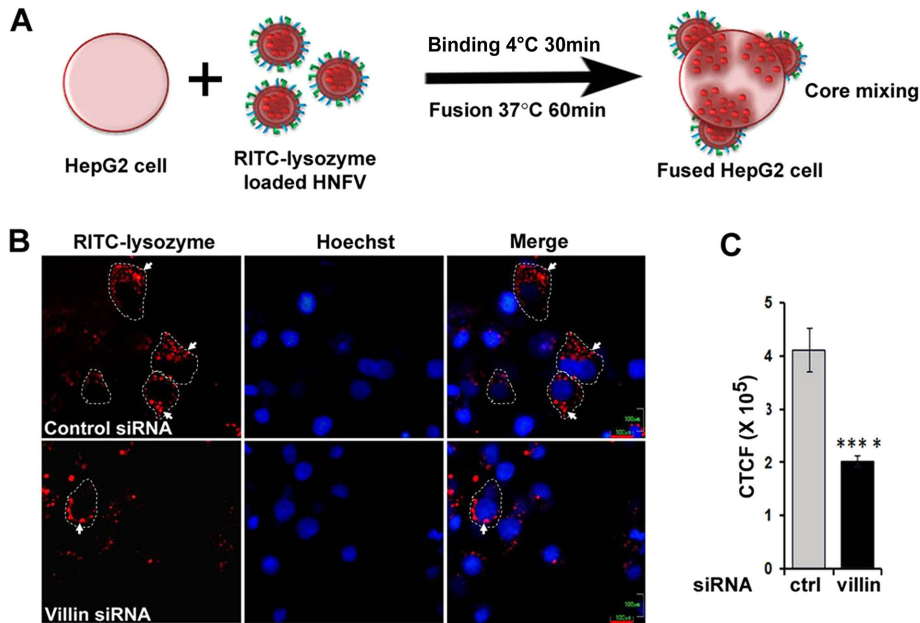
FIGURE 3: Villin affects HNFV-mediated complete fusion (core mixing). (A) Schematic depiction of workflow to monitor core mixing. (B) HepG2 cells transfected with control or villin-specific siRNA were allowed to bind and fuse with RITC-lysozyme–loaded HNFV and processed for microscopy. (C) CTCF (of RITC) expressed as mean ± SEM, $n = 25$. Arrows denote RITC-lysozyme in cytosol. Dotted lines denote boundaries of HNFV-fused cells. ****$p < 0.0001$; ctrl, control. Scale bars, 100 μm.

first and second rows). Until this point of fusion, however, villin-silenced cells did not show such cortical localization, confirming the role of villin in this process. An increase in overall F-actin, however, still could be observed throughout the cytosol as early as 5 min of fusion, suggesting F-actin synthesis is mainly induced by fusion and may not be due to a lack of villin's actin-severing function (Supplemental Figure S3C and Figure 5D, compare the third and fourth rows). We then quantified the total fluorescence intensity of F-actin and villin in HepG2 cells in the presence or absence of villin knockdown. As depicted in Figure 5E and Supplemental Figure S3D, the increase in F-actin in fusion samples is evident and corroborates with G/F-actin analysis of the same. Further quantification of F-actin in the cortical and cytoplasmic regions of cells during fusion (in comparison with control) showed a dramatic and significant redistribution of F-actin in the cortical regions during fusion (Figure 5F). It may be pointed out that during fusion, although villin colocalizes with actin at the cell cortex, its total cellular amount does not change significantly.

Next, to understand whether it is villin-induced polymerization of actin filaments that promotes fusion, we treated cells with jasplakinolide (JASP), a drug that polymerizes and stabilizes actin, and measured fusion kinetics with active virosomes. As expected, the presence of JASP caused a drastic increase in F-actin in these cells (Figure 5I) but, surprisingly, a decline in fusion (Figure 5J). Altogether, these experiments suggested that it is not the static polymerized F-actin but the dynamic rearrangement of actin that drives membrane fusion. Because villin-negative CHO cells also exhibit basal levels of HNFV-induced membrane fusion, we studied the role of cofilin, another ABP, in these cells. Interestingly, cofilin downregulation in CHO cells led to a decrease in fusion kinetics as well as extent (Figure 5, K and L), suggesting the role of alternative regulation of actin dynamics and membrane fusion in cells devoid of villin.

Villin regulates Sendai viral infection

Our results thus far have established that actin remodeling by villin plays an important role in Sendai virosome–cell fusion. Because membrane fusion is a key step for the entry of intact virus into the host cells (Knipe and Howley, 2013), we also investigated the role of villin in viral infection. Productive infection in the case of fusogenic enveloped viruses such as Sendai is reflected by syncytia formation and production of progeny viruses (Famulari and Fleissner, 1976; Lawton et al., 1986). As shown in Figure 6, A and B, syncytia formation is significantly dependent on villin. Progeny virus production was monitored by the appearance of viral proteins and production of functionally active virions in the infected cells. A direct correlation in the production of viral proteins, as monitored by viral protein-specific immunostaining, hemagglutination titer (expressed as hemagglutinating units [HAU]), hemolysis, and presence of Sendai F transcripts, with the level of villin expression (Figure 6, C–G) was observed. The appearance of viral proteins in infected cells decreased by ~2.51-fold in HepG2 cells devoid of villin (Figure 6D). Analysis of culture supernatant of infected host cells showed a sharp decline in viral yield in cells where villin was knocked down (hemolysis ~1.76-fold, Figure 6E, and HAU approximately fourfold, Figure 6F). To ascertain that such progeny virus formation was directly linked to fresh transcription of F gene in infected cells, quantitative PCR (qPCR) analysis was performed. As shown in Figure 6G, there was ~1.45-fold reduction of F transcripts in villin knockdown HepG2 cells. These findings and the core mixing assay (Figure 3) further strengthen our claim that villin definitely plays a role in virus-induced complete fusion (core mixing), ensuing syncytia formation, and production of progeny virus.

DISCUSSION

A complete virus–host membrane fusion encompasses the merging of viral and host lipid bilayers and fusion pore formation, followed by mixing of contents. During such an event, besides involvement of the lipid bilayer of host cells, subversion of the cytoskeletal meshwork of the inner membrane is also essential (Takimoto et al., 2001; Wurth et al., 2010; Grove and Marsh, 2011; Taylor, Koyuncu, and Enquist, 2011). However, a detailed profile of the host factors regulating such actin cytoskeletal modeling during membrane fusion is currently unknown. With an aim to understand this process, we used reconstituted Sendai viral envelopes (HNFV), which contain only viral lipids and membrane proteins and is the most appropriate physiological model to study the molecular mechanism of virus-induced membrane fusion (Bagai and Sarkar, 1993). A pioneer in providing an insight into virosome–host cell fusion-induced proteome alterations, our study reports the upregulation of villin, an ABP known to remodel actin cytoskeleton during several physiological and pathological processes, including bacterial invasions (Friederich et al., 1989; Ferrary et al., 1999; Athman et al., 2005; Tomar et al., 2006; Khurana and George, 2008; Lhocine et al., 2015). Two-dimensional immunoblots also revealed additional villin isoforms up-regulated during membrane
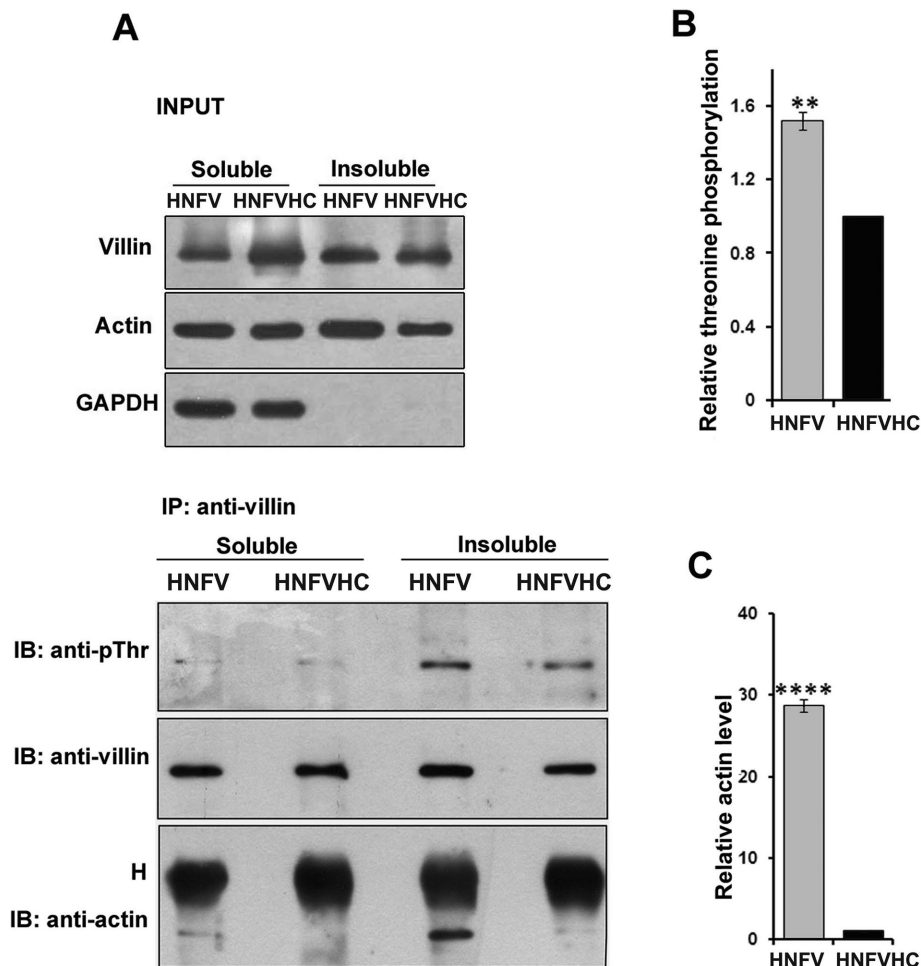
FIGURE 4: Membrane fusion strengthens the association of villin with actin. (A) From HepG2 cells 30 min postfusion with HNFV, Triton-soluble and -insoluble fractions were prepared as described in *Materials and Methods*. A portion of these fractions were either used as Input or were processed for coimmunoprecipitation using villin antibody and probed by Western blotting for phosphoantibodies, villin, actin, and GAPDH. Relative fold change of (B) threonine-phosphorylated villin and (C) actin, shown as mean ± SEM, $n = 5$. ** $p < 0.01$; **** $p < 0.0001$. H indicates immunoglobulin G heavy chain.

In the cytosol, actin exists as two different forms, globular monomeric G-actin and filamentous polymeric F-actin. Both polymerization and depolymerization of actin filaments constitute the basis of actin rearrangements. Biochemical and microscopic analysis of G/F-actin distribution in HepG2 cells exhibited an initial rapid decrease in G/F-actin ratio within 5 min of fusion. This was followed by a depolymerization of actin filaments, thus restoring the G-actin/F-actin balance within an hour. The sole effect of fusion could be envisaged because cells that were treated with heat-inactivated virosomes did not show any change in G/F-actin distribution. Microscopic analysis of villin and actin revealed that during fusion, villin is recruited to the cell cortex, close to the inner membrane bilayer. This suggests its active role in fusion via disruption of cortical actin cytoskeleton, which poses a mechanical barrier for the expansion of fusion pore in paramyxoviruses (Wurth *et al.*, 2010). A closer look at fused HepG2 cells revealed less polymerized actin in comparison with that of villin knockdown cells. The driving force that facilitates fusion is ultimately actin remodeling that includes both depolymerization and polymerization. In this respect, our experiment using JASP (which is known to stabilize F-actin and prevents actin remodeling) supports this notion. Treatment with JASP resulted in an increase in F-actin and a drastic decrease in the monomeric G-actin form. When such cells were subjected to interaction with virosomes, this resulted in a notable decrease in membrane fusion (Figure 5, I and J).

The colocalization and interaction of villin with actin during fusion bolsters our hypothesis that villin directs actin-based forces, thus alleviating the mechanical barrier to drive membrane fusion. Support of this concept can be drawn from our observation that in fused cells, actin actively interacts with villin at the cortical regions of the host cell. On the other hand, in absence of villin, actin meshwork is highly static, resulting in a lack of those forces and fine regulation of actin remodeling, culminating in abrogation of membrane fusion. Our work on actin remodeling during fusion showed an interesting pattern that initially during 5 min of fusion, villin induces actin polymerization. However, at the later stages of core mixing, villin seems to plays a different role in actin severing/capping, thus reducing the mechanical barrier and eventually supporting the steps of core mixing (Figure 5, A–H). To determine the essential role of actin remodeling during membrane fusion, we also attempted to investigate the possibility that other ABPs play a role in this process. Because SeV can fuse even in the absence of villin with villin-negative CHO cells (Shibata, Ishii, *et al.*, 2004; Das *et al.*, 2015), we compared their ability to fuse in the absence or presence of cofilin, another major ABP expressed in abundance in these cells. By knocking down cofilin gene expression, we found a drastic impairment of HNFV fusion compared with their fusion with control cells (Figure 5, K and L), thus

fusion in HepG2 cells, which corresponded to phosphorylation at threonine. The enhanced level of villin during fusion might be due to its increased stability through phosphorylation at threonine (Encinar *et al.*, 1998; Hong *et al.*, 2011; Nishi *et al.*, 2011).

Villin-induced enhancement of membrane fusion was verified in cells where villin expression was restricted by specific siRNAs. This drastically reduced virosome–host cell fusion as monitored by real-time fluorimetry. However, the lack of any effect of villin overexpression on HNFV–HepG2 fusion (Figure 2, G and H) suggested a lower threshold of villin is required for inducing membrane fusion. Although all our functional validations have been carried out using fusion assays monitoring membrane mixing of lipid probe Rhod-PE (hemifusion), this truly represents core mixing in the case of Sendai viral glycoprotein-mediated fusion (Verma, Mani, Sharma, *et al.*, 2005; Krishnan, Verma, *et al.*, 2009). However, to ensure this in the present context, the effect of villin on the delivery of RITC-lysozyme by HNFV (Figure 3) was examined and found to be in agreement with the results obtained by hemifusion assays, furthering our conviction that villin promotes complete membrane fusion.
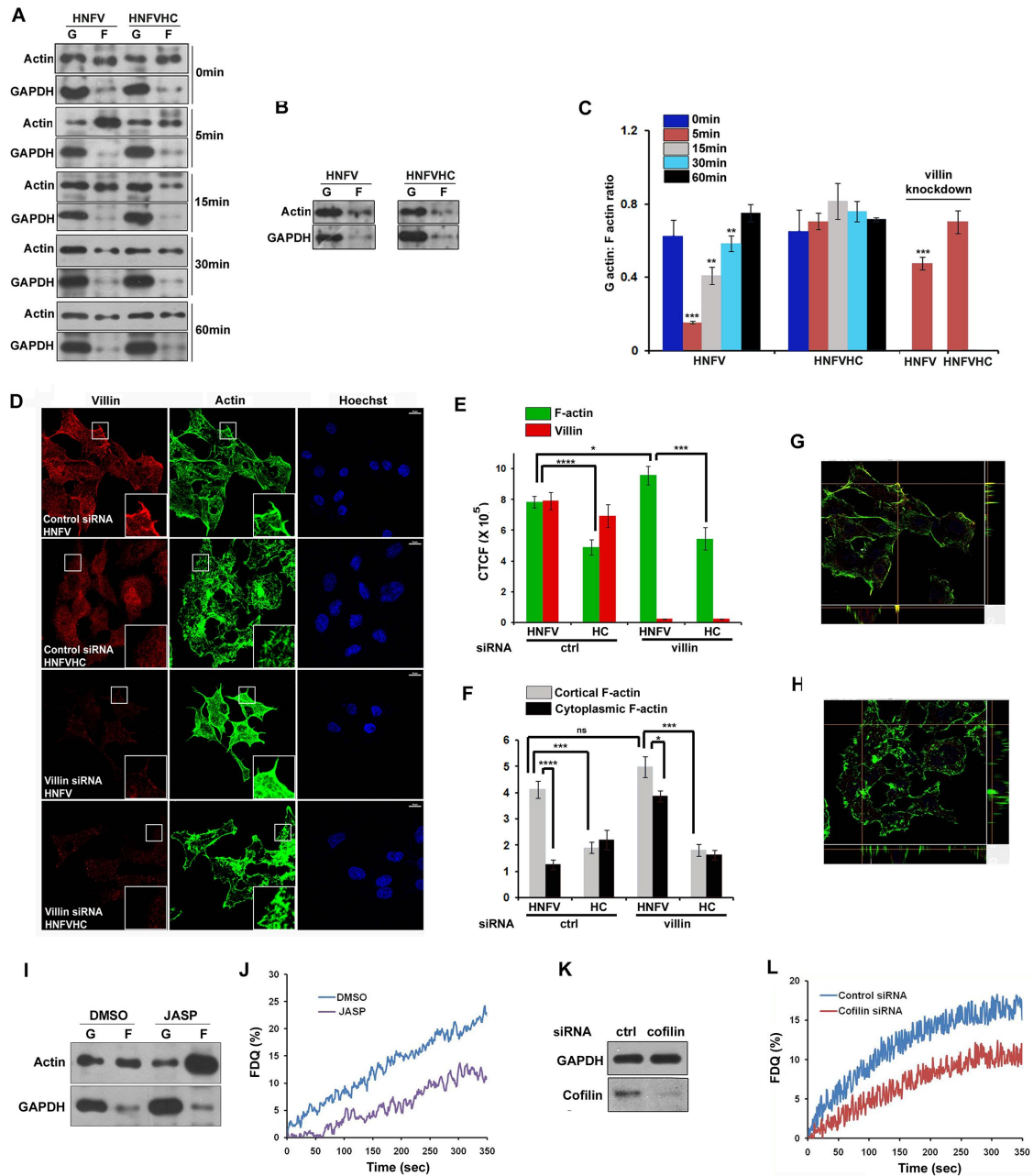
FIGURE 5: Villin modulates membrane fusion by altering the G/F-actin ratio. (A) HepG2 cells subjected to fusion with HNFV or HNFVHC (control) at 0 (no fusion, only binding), 5, 15, 30, and 60 min were processed for G- and F-actin analysis. G- and F-actin fractions were loaded on the gel and immunoblotted for actin and GAPDH. (B) Villin-depleted HepG2 cells were allowed to fuse with HNFV or HNFVHC for 5 min and subjected to G- and F-actin analysis. (C) Normalized data from A and B are expressed as mean ± SEM, $n = 5$. (D) HepG2 cells transfected with control or villin-specific siRNA were allowed to fuse with HNFV or HNFVHC (control) for 15 min. Fused cells were fixed, permeabilized, immunostained for villin, stained with BODIPY-phalloidin, and processed for confocal microscopy. Top view of Z-stacks is shown. (E) Quantification of total fluorescence intensity of F-actin (green bars) and villin (red bars) of cells in D. (F) Quantification of F-actin in cortical and cytoplasmic regions of cells in D. CTCF in E and F expressed as mean ± SEM, $n = 25$. (G, H) View along the XZ and YZ axes for the first and second rows of D, respectively. (I) G-actin/F-actin analysis of cells treated with JASP. (J) JASP-treated cells were allowed to bind with Rhod-PE–labeled HNFV (RhoHNFV), followed by measurement of fusion kinetics. Extent of fusion was recorded as the percentage of FDQ. Individual spectrum represents online recorded FDQ of one of the three independent experiments. (K) Immunoblot to confirm cofilin expression in HepG2 cells after transfection with control or cofilin-specific siRNA. (L) Cofilin-depleted HepG2 cells allowed to bind with Rhod-PE–labeled HNFV (RhoHNFV), followed by measurement of fusion kinetics. Extent of fusion was recorded as the percentage of FDQ. Individual spectrum represents online recorded FDQ of one of the three independent experiments. ****$p < 0.001$; ***$p < 0.001$; **$p < 0.01$; *$p < 0.05$; ns, not significant. Scale bars, 10 μm. ctrl, control.
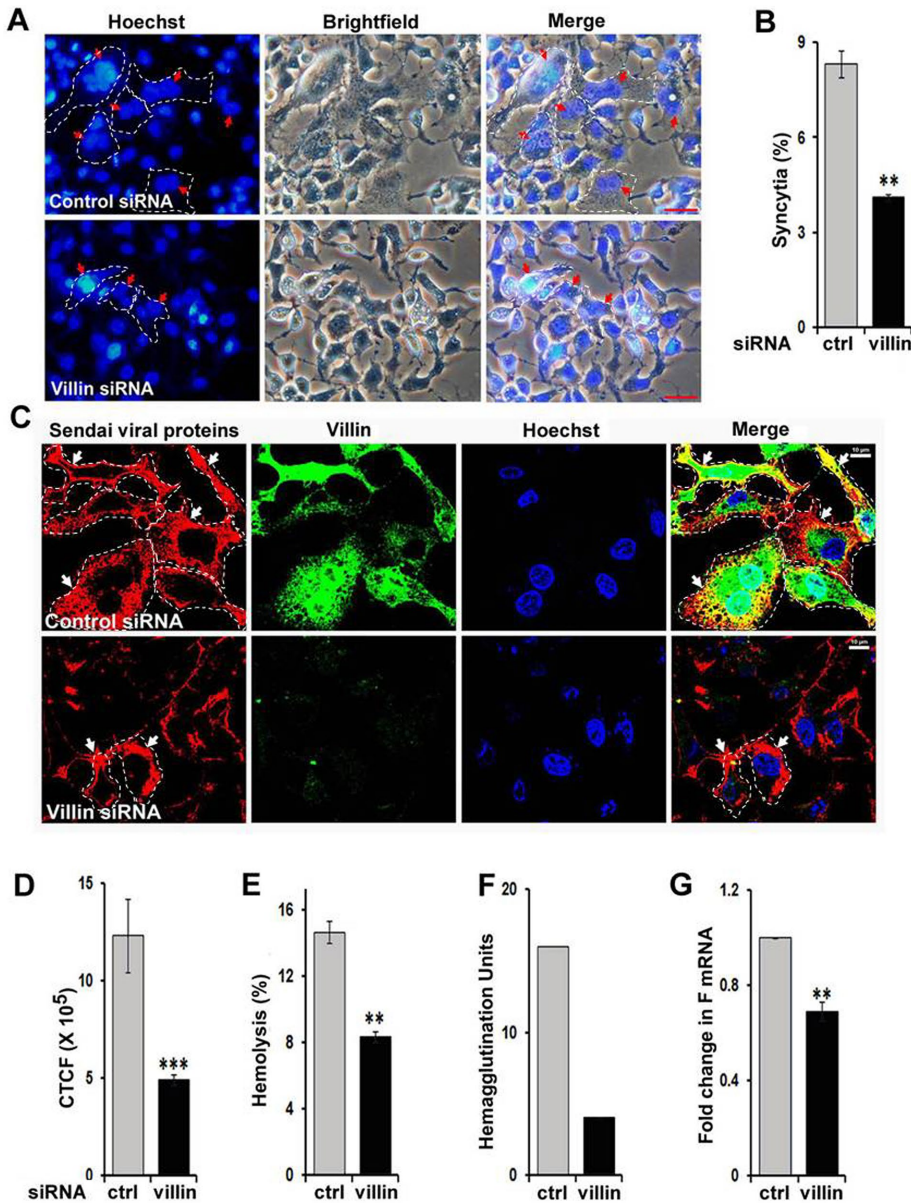
FIGURE 6: Villin enhances SeV-mediated syncytia formation, infection, and production of progeny virus. (A) HepG2 cells were transfected with control or villin-specific siRNA. Cells were infected with 400 HAU SeV at 72 h posttransfection. At 24 h postinfection, cells were fixed and examined under microscope. Syncytium is denoted by red arrows. Scale bars, 100 μm. (B) Percentage syncytia expressed as mean ± SEM, $n = 25$. (C) HepG2 cells transfected with control or villin-specific siRNA were subject to infection with SeV (400 HAU). At 24 h postinfection, cells were fixed, permeabilized, and immunostained with villin antibody (Alexa 488–conjugated 2° antibody) followed by antibody against SeV envelope glycoproteins (tetramethylrhodamine isothiocyanate–conjugated 2° antibody) and processed for confocal microscopy. Scale bars, 10 μm. (D) CTCF expressed as mean ± SEM, $n = 25$. Culture supernatant from cells in C was collected and assayed for (E) hemolysis and (F) hemagglutination titer. (G) In a parallel experiment, cells as in C were processed for RNA isolation and qPCR was performed for F mRNA expression. Data are expressed as mean ± SEM, $n = 5$. Arrows denote SeV envelope glycoproteins (F and HN). Dotted lines denote boundaries of infected cells. ***$p < 0.001$; **$p < 0.01$; ctrl, control.

(Takimoto et al., 2001). Accumulation and colocalization of F-actin with villin at the cell cortex indicates increased association of the two during fusion. F-actin binding sites in villin have been identified in the core (responsible for actin severing) and the headpiece (for actin bundling) by previous studies (Khurana, 2006). Future work should focus on working with mutants for such sites in the context of HNFV–host cell fusion.

Interestingly, threonine phosphorylation of villin in HepG2 cells led us to speculate about the possible involvement of MAPK pathways, as our earlier work suggested that this pathway mediates regulation of virosome–HepG2 cell fusion (Sharma et al., 2010). To identify the site of phosphorylation, immunoprecipitation followed by LC-MS/MS was performed that revealed threonine at the 206 position to be phosphorylated during fusion. This was supported by in silico analysis as well.

Expression of viral proteins and transcripts of F gene, along with dose-dependent enhancement of syncytia formation, confirm our claim that villin induces cytoskeletal remodeling during the infection process (Figure 6), and these results are in agreement with the opinions expressed in a review by Taylor, Koyuncu, and Enquist (2011). To summarize our findings based on an integration of the salient features depicting villin–actin interaction, we propose a model (Figure 7) demonstrating the role of villin and its interacting partners in the regulation of membrane fusion–mediated entry. So far our approach shows two aspects of villin's role during fusion: its phosphorylating modulation and its function to promote virosome fusion. It seems villin starts to play its important role during fusion right from the initial steps of lipid mixing (Figure 2). The observed modulated villin protein levels and its phosphorylation during the later course of fusion (Figure 1) may be due to signaling induced by initial lipid mixing as observed by us previously (Sharma et al., 2010). This idea may be in agreement with the studies showing that a MAPK pathway regulates villin expression (Cheung et al., 2011). Whether villin's phosphorylation and function are linked would be an interesting question to address to follow up this study.

Overall, these observations help us understand a novel but complex relationship of host cell factors during viral infection. It also brings to the forefront the importance of actin cytoskeleton and its regulatory elements in promoting viral entry. A recent perspective highlights the role of a diverse repertoire of various ABPs that function synergistically in a common cytoplasm to control actin dynamics and

suggesting an explicit role of ABP and cytoskeletal rearrangements to mediate membrane fusion with Sendai virosomes.

It is interesting to note that the cytoplasmic tail of F protein contains a sequence similar to that of an ABP and may bind to actin, driving membrane fusion through cytoskeletal rearrangements
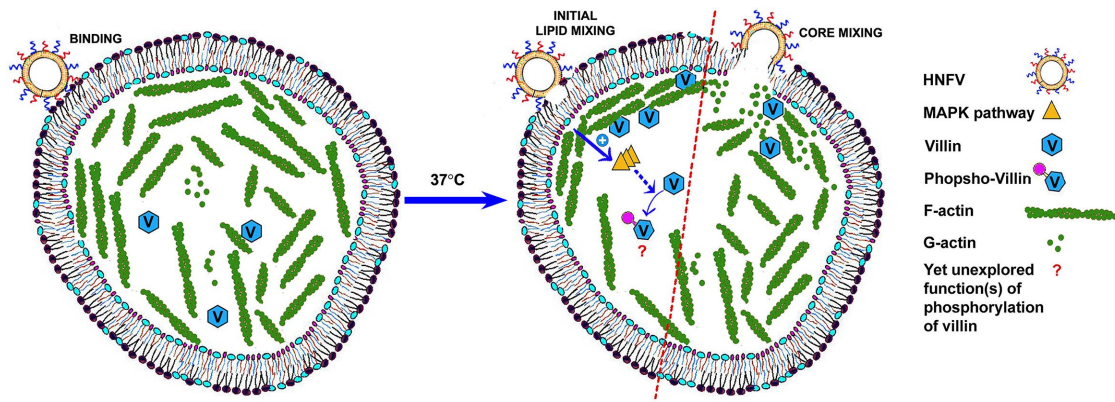
FIGURE 7: Proposed model depicting villin–actin interplay during virosome–cell fusion. In host cells, membrane fusion induces activation of MAPK pathways that, in turn, phosphorylates endogenous villin at threonine 206. During the initial event of membrane fusion (lipid mixing), villin colocalizes with actin at the cell cortex. Subsequently, during the later stages of core mixing, villin induces actin severing that reduces cortical barrier so as to facilitate viral entry.

cellular structure (Lappalainen, 2016). Our data on nonpathogenic SeV may be applicable to other related pathogenic enveloped viruses. Importantly, this information can be extended to improve the efficiency of our Sendai immuno-virosome–mediated targeted anti-cancer drug delivery to villin-negative cells (Kumar et al., 2015). Altogether, this study bears manifold consequences ranging from enrichment of knowledge on enveloped viral entry process and intracellular vesicular fusion to the formulation of efficient molecular therapeutics.

MATERIALS AND METHODS

Cell culture and SeV propagation
Human liver cell line HepG2 and CHO were obtained from the American Type Culture Collection (ATCC) and maintained in ATCC-recommended media and supplements (Sharma et al., 2010). Both cell lines were checked for interspecies cross-contamination and authenticated by Lifecode Technologies Pvt. (New Delhi, India). SeV (Z strain; obtained from Abraham Loyter, Hebrew University of Jerusalem, Israel) was grown in the allantoic sacs of 10-d-old embryonated chicken eggs. The virus was harvested and purified according to standard procedures as previously reported (Bagai et al., 1993).

Reagents and biologicals
L-α-Phosphatidylethanolamine-N-(lissamine rhodamine B sulfonyl) (ammonium salt, egg-transphosphatidylated) (Rhod-PE, 810146) was purchased from Avanti Polar Lipids (Alabaster, AL). SM2 Bio-Beads were obtained from Bio-Rad (Hercules, CA). Triton X-100 (TX-100) was obtained from Aldrich (St. Louis, MO). Cell culture reagents and Dulbecco's phosphate-buffered saline (DPBS) were procured from Invitrogen (Carlsbad, CA). Protease inhibitor cocktail (P8340), phosphatase inhibitor cocktails 2 (P5726) and 3 (P0044), Protein A-Sepharose CL4B (P3391), sodium azide (S2002), and 4-(2-hydroxyethyl)-1-piperazineethanesulfonic acid (HEPES; H4034) were purchased from Sigma (St. Louis, MO). Prolong Diamond Antifade (P36961), BODIPY FL Phallacidin (B607), and a glycoprotein staining kit (24562) were purchased from Molecular Probes (Eugene, OR). All reagents used for 2D electrophoresis were purchased from GE Healthcare (Little Chalfont, UK). FOCUS FASTsilver staining kit for preparative gel was purchased from G-Biosciences (St. Louis, MO). Reagents for in-gel digestion were of mass spectrometry grade and obtained from Fluka (St. Louis, MO).

Antibodies
The antibodies used for Western blotting and coimmunoprecipitation assays are listed in Supplemental Table S2.

Plasmid constructs
Plasmid expressing GFP-tagged villin was obtained from Origene (RG216340).

Preparation of virosomes (HNFV)
Reconstituted Sendai viral envelopes, known as virosomes, were prepared using standard procedures established in our lab. Briefly, HNFV was prepared by directly solubilizing the Sendai viral envelope with Triton X-100. This was followed by removal of Triton using SM2 Bio-Beads and ultracentrifugation to obtain the virosome, which was then resuspended in 1× DPBS. For fluorescence labeling, the supernatant obtained after Triton treatment was incubated in a Rhod-PE–coated glass tube (coated under N_2 gas) for 30 min at room temperature (RT) and then subjected to ultracentrifugation to finally obtain the Rho-virosomes in the pellet. Virosomes were suspended in 1× phosphate-buffered saline and tested for their functional activity using hemagglutination and hemolysis assays (Bagai et al., 1993).

Transfection
HepG2 cells (grown on coverslips in six-well plates) at 50–60% confluency were transfected with 1 μg plasmid DNA using Lipofectamine LTX and Plus reagent (Invitrogen, Carlsbad, CA) and were processed 48 h posttransfection for functional assays. OptiMEM I was used for preparation for DNA-lipid complex. Sixty picomol of villin siRNA (L-012383-00-0010, SMARTpool ON-TARGETplus siRNA) or GFP siRNA (P-002048-01-20, used as control or nonspecific siRNA) obtained from Dharmacon (Lafayette, CO) was transfected in HepG2 cells using Lipofectamine RNAiMax (Invitrogen, Carlsbad, CA) and processed after 72 h of incubation. In case of cofilin siRNA (P-002048-01-20), 200 pmol of siRNA was used, obtained as SMARTpool ON-TARGETplus siRNA from Dharmacon (Lafayette, CO). For kinetic assays, cells were grown in 100-mm dishes, and the amount of cDNA construct/siRNA was increased accordingly.

Immunofluorescence and confocal microscopy
Virosomes (10 μg) were added to cells (grown in coverslips) on a six-well plate and allowed to bind for 30 min at 4°C. The cells were

washed and reincubated in prewarmed media at 37°C for 15 min. Thereafter, cells were fixed with 4% paraformaldehyde, permeabilized with 0.5% Triton/1% Tween 20, and blocked with 2% bovine serum albumin (BSA). Next, immunodetection was performed using fluorescently labeled antibodies as mentioned in Supplemental Table S2. For visualization of actin, staining with BODIPY-conjugated phalloidin was performed according to the manufacturer's protocol. Nuclei were counterstained with Hoechst, after which the coverslips were mounted onto a clean glass slide using Prolong Diamond Antifade. Images were captured with a Plan Apo VC 60× oil differential interference contrast microscopy (DIC) N2 objective on a Nikon A1 inverted confocal laser-scanning microscope. The fluorophores were excited by lasers having wavelengths of 405, 488, and 543 nm, and the emissions were detected using detectors with sensitivity spectra of 425–475, 500–530, and 552–670 nm, respectively. Images were analyzed using NIS-Elements Advanced Research imaging software (version 3.22.00). Cell fluorescence was quantified by calculating corrected total cell fluorescence (CTCF) using ImageJ software (National Institutes of Health); CTCF = integrated density – (area of selected cell × mean fluorescence of background readings). For F-actin distribution analysis, CTCF values obtained from several selected areas in the cortical regions of each cell were plotted against that of the inner cytoplasmic regions of the same cell.

Fusion of HNFV with HepG2

HepG2 cells were serum starved for 14 h and treated with sodium azide (10 mM) for an hour, at 37°C. RhoHNFV (30 µg) and a corresponding amount of HNFVHC (virosomes heat inactivated at 56°C for 30 min) were added to the monolayer cells in separate flasks and incubated at 4°C for 30 min for binding. Cells were then washed with prewarmed media and further incubated at 37°C for 30 and 60 min of fusion, as indicated elsewhere.

Sample preparation for proteomics

HepG2 cells were lysed in DIGE lysis buffer (7 M urea, 2 M thiourea, 4% 3-[(3-cholamidopropyl)dimethylammonio]-1-propanesulfonate hydrate [CHAPS], 30 mM Tris, pH 8.5) containing 1% phosphatase inhibitor and protease inhibitor cocktails. Lysing was followed by sonication (amplitude 50%, pulse on: 4 s, pulse off: 59 s, for a total time of 30 s). The final cell extracts were obtained after centrifugation at $17,000 \times g$ for 30 min at 4°C and stored in aliquots at –80°C. Protein concentration was determined using a modified Bradford assay (Ramagli and Rodriguez, 1985). Fifty micrograms of each sample (per immobilized pH gradient [IPG] strip per sample) was used for 2D-DIGE, 500 µg of each was used for preparative gel and mass spectrometry, and 75 µg each was used for 2D immunoblotting.

DIGE, image analysis, and protein identification

Cell lysates were labeled with the CyDye DIGE Fluor minimal dyes (GE Healthcare, Little Chalfont, UK) according to the manufacturer's protocol. Working dye solution (1 µl; 400 pmol/µl) in anhydrous dimethylformamide was added to 50 µg of each protein sample and vortexed. After a brief centrifugation, the samples were incubated on ice for 30 min in the dark. The reaction was terminated by the addition of 1 µl of 10 mM lysine, and the samples were kept on ice in the dark for 10 min. Fusion samples of 30 min, 60 min, and control (HNFVHC), including biological replicates, were labeled with Cy3 and Cy5. A dye swap for each set of samples was done to avoid dye bias. An internal standard, a pool of equal amounts of protein from all samples, was labeled with Cy2. The Cy2-, Cy3-, and Cy5-labeled samples were pooled according to the experimental setup (Supplemental Table S3). An appropriate volume of DIGE rehydration

solution (7 M urea, 2 M thiourea, 4% CHAPS, and 0.002% bromophenol blue) with 0.2% dithiothreitol (DTT) and 2% ampholytes (nonlinear pH 3–10) was added to the sample. The protein mixture was then rehydrated on 24-cm-long IPG strips, nonlinear pH 3–10, at RT for 16–18 h. Subsequently, the first dimensional separation or isoelectric focusing (IEF) was performed at 20°C using the Ettan IPGphor 3 IEF system (GE Healthcare, Little Chalfont, UK) according to the manufacturer's recommendation. For 2D-immunoblotting, 13-cm IPG strips were used and IEF was performed accordingly. The focused IPG strips were then subject to reduction with 1% DTT in 10 ml of equilibration buffer (6 M urea, 75 mM Tris-base, 2% SDS, 29.3% glycerol, and 0.002% bromophenol blue) for 20 min, followed by alkylation with 2.5% iodoacetamide in the same buffer for another 20 min. Thereafter, the strip was placed onto a 12% polyacrylamide slab gel (18 × 16 cm) and sealed with 0.5% agarose in SDS running buffer. The second dimensional separation was performed in an Ettan Dalt Six Electrophoresis Unit until the bromophenol blue dye reached the end of the gel. The 2D-DIGE images were acquired by scanning the gels using a Typhoon Trio variable-mode imager (GE Healthcare, Little Chalfont, UK) at a 100-µm pixel size resolution. The excitation/emission wavelengths for Cy2, Cy3, and Cy5 were 488/520, 532/580, and 633/670 nm, respectively. The resulting DIGE images were analyzed using DeCyder software version 7.0 (GE Healthcare, Little Chalfont, UK). The gels were analyzed in both difference in-gel analysis (DIA) and biological variance analysis (BVA) modes. The Cy2 internal standard allowed normalization of data across two or more gels. For each set of experiments, there were six DIAs included in one BVA. In BVA, statistical analysis using Student's t test was performed, and the spots of significant differential expression ($p \leq 0.02$) were chosen. By considering 3D spot contour, fold difference, clustering of data points in graph, and position in the gel, some protein spots were marked as "proteins of interest" for further analysis. For determining the identity of the differentially expressed protein spots, a preparative gel was run with 500 µg protein. Except for the fact that here no CyDye labeling is required, the rest of the protocol including rehydration, IEF, and second dimensional separation were the same as mentioned previously. After the second-dimension SDS–PAGE, the gels were subject to silver staining with the FOCUS FASTsilver kit (G-Biosciences, St. Louis, MO), and the gel image was incorporated into DeCyder analysis for matching with the analytical gels. Spots to be picked up were identified in the preparative gel, which was subject to spot picking manually. The protein spots thus picked up were subject to in-gel digestion. The silver-stained gel pieces were destained with 15 mM potassium ferricyanide and 50 mM sodium thiosulfate (1:1). This was followed by washing with 50 mM ammonium bicarbonate (ABC) and acetonitrile (1:1) and drying of the solution by speed vac. Thereafter, 20 µl of DTT solution (10 mM DTT in 100 mM ABC) was added to the sample and incubated at 60°C for 30 min. The supernatant so obtained was then discarded, and the gel piece was washed with wash solution (50% ABC and 50% acetonitrile). The solution was again dried by speed vac. Then, 20 µl of iodoacetamide solution (55 mM IAA in 100 mM ABC) was added, and the resulting solution was incubated at RT for 45 min in the dark. The supernatant obtained was discarded, and the gel piece was washed again with wash solution, followed by drying by speed vac. Thereafter, 100% acetonitrile was added, after which the gel piece was allowed to dry completely. This was followed by the addition of 20 µl of working solution of trypsin (12.5 ng/µl in 50 mM ABC). The gel pieces were incubated in ice for 30 min, until swollen. Next, 20 µl of 10 mM ABC was added, followed by overnight incubation at 37°C. The solution was cooled down to RT, and the supernatant was directly removed into a fresh

tube. Extraction of peptides was done with the addition of 20–50 μl of 50% acetonitrile and 1% formic acid and incubation for 5 min at RT. After vortexing, the supernatant was collected, desalted, and concentrated using C18 Ziptip (Millipore, Billerica, MA) and processed for mass spectrometry.

Coimmunoprecipitation

HepG2 cells were allowed to bind and fuse with virosomes as described above. Cell lysates were extracted with lysis buffer containing 20 mM HEPES (pH 7.2), 1% Triton, and 150 mM NaCl supplemented with 1% protease and phosphatase inhibitor cocktails for 30 min at 4°C and subsequently centrifuged at $6200 \times g$ for 4 min at 4°C, and the supernatant was collected as the Triton-soluble fraction (Sol.). The pellet was resuspended in buffer containing 15 mM HEPES (pH 7.5), 150 mM NaCl, 1% Triton, 1% sodium deoxycholate, 0.1% SDS, and 10 mM EDTA and supplemented with 1 mM DTT and 1% protease and phosphatase inhibitor cocktails. This was centrifuged at $17,000 \times g$ for 20 min at 4°C, and the supernatant represented the Triton-insoluble pool (Insol.). Both extracts (1 mg each) were immunoprecipitated with anti-villin antibody. The immunoprecipitates were analyzed on 10% SDS–PAGE and immunoblotted with antibodies for phosphotyrosine, phosphothreonine, phosphoserine, villin, and actin.

Western blotting

Cell lysates were resolved by 10 or 12% SDS–PAGE and transferred onto nitrocellulose or polyvinylidene difluoride membrane. Following transfer, the membrane was blocked with 2% BSA in Tris-buffered saline (TBS) (pH 7.4) containing 0.05% Tween 20 for 1 h at RT and then incubated with primary antibody at 4°C overnight, followed by washings in TBS with 0.1% Tween 20. This was followed by incubation with horseradish peroxidase–conjugated secondary antibody for 1 h at RT and washings with TBS. Chemiluminescence signals were visualized by an enhanced chemiluminescence (ECL) detection system and captured on Kodak film (ECL hypersensitive film in case of coimmunoprecipitation and 2D blots).

G-actin F-actin assay

The amount of G-actin and F-actin was determined using the G-actin/F-actin in vivo assay kit from Cytoskeleton (Denver, CO) according to the manufacturer's instructions. Briefly, cells were lysed, and the lysate was centrifuged at $100,000 \times g$ for 1 h at 37°C. The supernatants contained G-actin, whereas the pellet contained F-actin. Samples were subject to 10% SDS–PAGE followed by immunoblotting with actin and GAPDH antibodies. Quantification was done by determining the G/F-actin ratio for each sample, after normalization with respect to GAPDH.

Kinetics of virosome fusion with HepG2 cells (lipid mixing)

HepG2 cells ($\sim 4 \times 10^6$) were transfected with cDNA/siRNA (as indicated in the text) and incubated with 10 μg of Rho-virosomes for 40 min at 4°C. Cells were centrifuged at $0.5 \times g$ for 5 min to remove unbound virosomes, and the pellet was suspended in 100 μl of 10 mM cold DPBS. For measuring fusion kinetics, 50 μl of the labeled HNFV–cell complex suspension was placed in a cuvette containing 3 ml of prewarmed DPBS. Kinetics of fusion was recorded online by a spectrofluorimeter (FL3-22; Horiba). The percentage of FDQ at any time point was calculated according to the following equation:

% FDQ = $[(F - F_0)/F_t - F_0)] \times 100$

where F is FDQ, F_0 is FDQ at time zero, and F_t is FDQ post–Triton X-100 addition (Bagai et al., 1993).

Cytosolic delivery of RITC-lysozyme into cells (core mixing)

Control siRNA– or villin siRNA–transfected HepG2 cells were incubated with RITC-lysozyme–loaded HNFV for 30 min in serum-depleted media. Unbound HNFV were washed off, and cells were further incubated in complete media for 1 h, followed by visualization using an epifluorescence microscope (Nikon TE300 Eclipse).

SeV infection, syncytia assay, and analysis of progeny virus

Transfected HepG2 cells were infected with 400 HAU SeV. Cells were allowed to bind to SeV for 45 min at RT, and thereafter, media was replaced with serum containing media and kept at 37°C. Twelve hours after infection, cells were visualized for syncytia using Hoechst stain. For analysis of progeny virus, culture supernatant of infected cells was subjected to hemagglutination and hemolysis assays using human red blood cells (Bagai et al., 1993). Immunofluorescence for Sendai viral envelope proteins was performed on cells grown on coverslips as mentioned above.

RNA isolation and real-time reverse-transcription qPCR

Total RNA was extracted from cells using Trizol (according to the manufacturer's instructions). RNA (1 μg) was subject to reverse transcription using Moloney murine leukemia retrovirus (MMLV) reverse transcriptase (Fermentas). The resulting cDNA was amplified using primers specific for villin or Sendai F gene. The sequences of the primers used for PCR were as follows:

Villin: Forward primer 5′ TTGTCCTCAAGACCCAGT 3′
Reverse primer 5′ AGATGGTGTCAGCAACCA 3′
Sendai F: Forward primer 5′ CAGGGATTGCACTAGCCGAA 3′
Reverse primer 5′ GAATTTGTTCCCCCACAGCG 3′

In silico deduction of p-threonine site of villin

The conservation at each of the 46 threonine residues in villin was analyzed using the ConSeq (Berezin et al., 2004) server. Homologues were retrieved from UNIREF90 using the CS-BLAST algorithm with three iterations, an E-value cutoff of 0.0001, and a minimum sequence identity of 25%. Sequences were then clustered at 90% sequence identity to remove any redundancy in the data set and then aligned. By assessing the evolutionary rate and solvent accessibility at individual residue positions, ConSeq scores the residues based on the predicted functional importance. Eleven threonine residues with a ConSeq score of less than –0.5 were considered for further analyses. Then, all known cases of threonine phosphorylation of villin as determined by experimental techniques were considered using the online system biology resource PhosphoSitePlus (Hornbeck et al., 2012).

Detection of phosphorylated sites

Cell extracts subject to fusion with virosomes were processed for immunoprecipitation by villin, followed by in-gel digestion of the immunoprecipitated protein and mass spectrometry. LC-MS/MS was performed using a Thermo Q-Exactive mass spectrometer interfaced with a nanoflow LC system (Easy nLC II; Thermo Scientific). Peptides were separated on a Bio Basic C18 pico-Frit nanocapillary column (75 μm × 10 cm; New Objective, Woburn, MA) using a 60-min linear gradient of the mobile phase (5% acetonitrile containing 0.2% formic acid [buffer-A] and 95% acetonitrile containing 0.2% formic acid [buffer-B]) at a flow rate of 300 nl/min. Full-scan mass spectrometry spectra ($m/z = 400$–2000) were acquired after accumulation to a target value of 1e^6 ions with resolution of $r = 60,000$. MS/MS analysis was performed by selecting the top 20 peptides. Data files were analyzed using SEQUEST with a peptide mass tolerance of 5 ppm and a fragment mass tolerance of 0.05 Da. Potential sites of modification must meet the minimum criteria of a peptide

probability of 1.0 E^{-3} or better and have an Xcorr versus charge state >2.0, 2.3, and 2.8 for +1, +2, and +3 ions. All phosphorylation site identifications were confirmed by manual inspection of the raw data.

Statistical analysis

All experiments were performed in triplicate and the results were compared with appropriate controls using unpaired Student's *t* test. For proteomic experiments, fold difference with $p < 0.02$ were considered significant. All microscopic images were processed by calculating CTCF (as mentioned earlier in the text), and for each data analysis, and the p values are mentioned in the figure legends. These experiments were repeated five times and results were comparable. FDQ analysis was done in triplicate and a representative graph has been shown.

REFERENCES

Boldface names denote co–first authors.

Athman R, Fernandez MI, Gounon P, Sansonetti P, Louvard D, Philpott D, Robine S (2005). Shigella flexneri infection is dependent on villin in the mouse intestine and in primary cultures of intestinal epithelial cells. Cell Microbiol 7, 1109–1116.

Athman R, Louvard D, Robine S (2003). Villin enhances hepatocyte growth factor-induced actin cytoskeleton remodeling in epithelial cells. Mol Biol Cell 14, 4641–4653.

Bagai S, Lamb RA (1996). Truncation of the COOH-terminal region of the paramyxovirus SV5 fusion protein leads to hemifusion but not complete fusion. J Cell Biol 135, 73–84.

Bagai S, Puri A, Blumenthal R, Sarkar DP (1993). Hemagglutinin-neuraminidase enhances F protein-mediated membrane fusion of reconstituted Sendai virus envelopes with cells. J Virol 67, 3312–3318.

Bagai S, Sarkar DP (1993). Reconstituted Sendai virus envelopes as biological carriers: dual role of F protein in binding and fusion with liver cells. Biochim Biophys Acta 1152, 15–25.

Bagai S, Sarkar DP (1994). Fusion-mediated microinjection of lysozyme into HepG2 cells through hemagglutinin neuraminidase-depleted Sendai virus envelopes. J Biol Chem 269, 1966–1972.

Berezin C, Glaser F, Rosenberg J, Paz I, Pupko T, Fariselli P, Casadio R, Ben-Tal N (2004). ConSeq: The identification of functionally and structurally important residues in protein sequences. Bioinformatics 20, 1322–1324.

Blumenthal R, Loyter A (1991). Reconstituted viral envelopes—"Trojan horses" for drug delivery and gene therapy? Trends Biotechnol 9, 41–45.

Bretscher A, Weber K (1980). Villin is a major protein of the microvillus cytoskeleton which binds both G and F actin in a calcium-dependent manner. Cell 20, 839–847.

Cheung R, Kelly J, Macleod RJ (2011). Regulation of villin by Wnt5a/Ror2 signaling in human intestinal cells. Front Physiol 2, 58.

Corte AD, Maugeri N, Pampuch A, Cerletti C, de Gaetano G, Rotilio D (2008). Application of 2-dimensional difference gel electrophoresis (2D-DIGE) to the study of thrombin-activated human platelet secretome. Platelets 19, 43–50.

Das P, Saha S, Chandra S, Das A, Dey SK, Das MR, Sen S, Sarkar DP, Jana SS (2015). Phosphorylation of nonmuscle myosin II-A regulatory light chain resists Sendai virus fusion with host cells. Sci Rep 5, 1–15.

Eltoweissy M, Dihazi GH, Müller GA, Asif AR, Dihazi H (2016). Protein DJ-1 and its anti-oxidative stress function play an important role in renal cell mediated response to profibrotic agents. Mol BioSyst 12, 1842–1859.

Encinar JA, Fernandez A, Ferragut JA, Gonzalez-Ros JM, DasGupta BR, Montal M, Ferrer-Montiel A (1998). Structural stabilization of botulinum neurotoxins by tyrosine phosphorylation. FEBS Lett 429, 78–82.

Famulari NG, Fleissner E (1976). High-titer replication of nondefective Sendai virus in MDBK cells. J Virol 17, 597–604.

Ferrary E, Cohen-Tannoudji M, Pehau-Arnaudet G, Lapillonne A, Athman R, Ruiz T, Boulouha L, El Marjou F, Doye A, Fontaine JJ, et al. (1999). In vivo, villin is required for Ca2+ dependent F-actin disruption in intestinal brush borders. J Cell Biol 146, 819–830.

Friederich E, Huet C, Arpin M, Louvard D (1989). Villin induces microvilli growth and actin redistribution in tansfected fibroblasts. Cell 59, 461–475.

Gallo LI, Lagadari M, Piwien-Pilipuk G, Galigniana MD (2011). The 90-kDa heat-shock protein (Hsp90)-binding immunophilin FKBP51 is a mitochondrial protein that translocates to the nucleus to protect cells against oxidative stress. J Biol Chem 286, 30152–30160.

George SP, Chen H, Conrad JC, Khurana S (2013). Regulation of directional cell migration by membrane-induced actin bundling. J Cell Sci 126, 312–326.

Gerke V, Moss SE (2002). Annexins: from structure to function. Physiol Rev 82, 331–371.

Greber UF (2002). Signalling in viral entry. Cell Mol Life Sci 59, 608–626.

Grove J, Marsh M (2011). The cell biology of receptor-mediated virus entry. J Cell Biol 195, 1071–1082.

Harmon B, Ratner L (2008). Induction of the Galpha(q) signaling cascade by the human immunodeficiency virus envelope is required for virus entry. J Virol 82, 9191–9205.

Hong J, Zhou J, Fu J, He T, Qin J, Wang L, Liao L, Xu J (2011). Phosphorylation of serine 68 of twist1 by MAPKs stabilizes twist1 protein and promotes breast cancer cell invasiveness. Cancer Res 71, 3980–3990.

Hornbeck PV, Kornhauser JM, Tkachev S, Zhang B, Skrzypek E, Murray B, Latham V, Sullivan M (2012). PhosphoSitePlus: A comprehensive resource for investigating the structure and function of experimentally determined post-translational modifications in man and mouse. Nucleic Acids Res 40, 261–270.

Huang Q, Wang L, Bai S, Lin W, Chen W, Lin J, Lin X (2009). Global proteome analysis of Hepatitis B virus expressing human hepatoblastoma cell line HepG2. J Med Virol 81, 1539–1550.

Jin M, Szapiel N, Zhang J, Hickey J, Ghose S (2010). Profiling of host cell proteins by two-dimensional difference gel electrophoresis (2D-DIGE): Implications for downstream process development. Biotechnol Bioeng 105, 306–316.

Kemble GW, Danieli T, White JM (1994). Lipid-anchored influenza hemagglutinin promotes hemifusion, not complete fusion. Cell 76, 383–391.

Khurana S (2000). Role of actin cytoskeleton in regulation of ion transport: examples from epithelial cells. J Membr Biol 178, 73–87.

Khurana S (2006). Structure and function of villin. Adv Mol Cell Biol 37, 89–117.

Khurana S, George SP (2008). Regulation of cell structure and function by actin-binding proteins: Villin's perspective. FEBS Lett 582, 2128–2139.

Kim HS, Kim JS, Lee YK, Koo KH, Park YS (2008). An efficient liposomal gene delivery vehicle using Sendai F/HN proteins and protamine. Cancer Gene Ther 15, 214–224.

Knipe DM, Howley PM (eds.) (2013). Fields Virology, 6th Ed., Philadelphia, PA: Lippincott Williams & Wilkins.

Kondo T, Hirosashi S (2009). Application of 2D-DIGE in cancer proteomics towards personalized medicine. Methods Mol Biol 577, 135–154.

Krishnan A, Verma SK, Mani P, Gupta R, Kundu S, Sarkar DP (2009). A histidine switch in hemagglutinin-neuraminidase triggers paramyxovirus-cell membrane fusion. J Virol 83, 1727–1741.

Kumar M, Mani P, Pratheesh P, Chandra S, Jeyakkodi M, Chattopadhyay P, Sarkar DP, Sinha S (2015). Membrane fusion mediated targeted cytosolic drug delivery through scfv engineered sendai viral envelopes. Curr Mol Med 15, 386–400.

Lappalainen P (2016). Actin-binding proteins: the long road to understanding the dynamic landscape of cellular actin networks. Mol Biol Cell 27, 2519–2522.

Lawton P, Karimi Z, Mancinelli L, Seto JT (1986). Persistent infections with Sendai virus and Newcastle disease viruses. Arch Virol 89, 225–233.

Lhocine N, Arena ET, Bomme P, Ubelmann F, Prévost MC, Robine S, Sansonetti PJ (2015). Apical invasion of intestinal epithelial cells by salmonella typhimurium requires villin to remodel the brush border actin cytoskeleton. Cell Host Microbe 17, 164–177.

Luthra P, Sun D, Wolfgang M, He B (2008). AKT1-dependent activation of NF-kappaB by the L protein of parainfluenza virus 5. J Virol 82, 10887–10895.

Muroi M, Kazami S, Noda K, Kondo H, Takayama H, Kawatani M, Usui T, Osada H (2010). Application of proteomic profiling based on 2D-DIGE for classification of compounds according to the mechanism of action. Chem Biol 17, 460–470.

Nishi H, Hashimoto K, Panchenko AR (2011). Phosphorylation in protein-protein binding: Effect on stability and function. Structure 19, 1807–1815.

Okada Y (1988). Sendai virus-mediated cell fusion. Curr Top Membr Trans 32, 297–336.

Pleschka S, Wolff T, Ehrhardt C, Hobom G, Oliver P, R RU, Ludwig S (2001). Influenza virus propagation is impaired by inhibition of the Raf/MEK/ERK signalling cascade. Nat Cell Biol 3, 301–305.

Ramagli LS, Rodriguez LV (1985). Quantitation of microgram amounts of protein in SDS-mercaptoethanol-tris electrophoresis sample buffer. Electrophoresis 6, 559–563.

Ramani K, Hassan Q, Venkiah B, Hasnain S, Sarkar DP (1998). Site-specific gene delivery in vivo through engineered Sendai. Proc Natl Acad Sci USA 95, 11886–11890.

Sarkar DP, Morris SJ, Eidelman O, Zimmerbergl J, Blumenthal R (1989). Initial stages of influenza hemagglutinin-induced cell fusion monitored simultaneously by two fluorescent events: cytoplasmic continuity and lipid mixing. J Cell Biol 109, 113–122.

Sharma NR, Mani P, Nandwani N, Mishra R, Rana A, Sarkar DP (2010). Reciprocal regulation of AKT and MAP kinase dictates virus-host cell fusion. J Virol 84, 4366–4382.

Shendelman S, Jonason A, Martinat C, Leete T, Abeliovich A (2004). DJ-1 is a redox-dependent molecular chaperone that inhibits α-synuclein aggregate formation. PLoS Biol 2, 1764–1773.

Shibata M, Ishii J, Koizumi H, Shibata N, Dohmae N, Takio K, Adachi H, Tsujimoto M, Arai H (2004). Type F scavenger receptor SREC-I interacts with advillin, a member of the gelsolin/villin family, and induces neurite-like outgrowth. J Biol Chem 279, 40084–40090.

Sun J, Barbieri JT (2004). ExoS Rho GTPase-activating protein activity stimulates reorganization of the actin cytoskeleton through Rho GTPase guanine nucleotide disassociation inhibitor. J Biol Chem 279, 42936–42944.

Takimoto T, Murti KG, Bousse T, Ann Scroggs R, Portner A (2001). Role of matrix and fusion proteins in budding of sendai virus role of matrix and fusion proteins in budding of sendai virus. J Virol 75, 11384–11391.

Taylor MP, Koyuncu OO, Enquist LW (2011). Subversion of the actin cytoskeleton during viral infection. Nat Rev Microbiol 9, 427–439.

Tomar A, George S, Kansal P, Wang Y, Khurana S (2006). Interaction of phospholipase C-gamma1 with villin regulates epithelial cell migration. J Biol Chem 281, 31972–31986.

Verma SK, Mani P, Sharma NR, Krishnan A, Kumar VV, Reddy BS, Chaudhuri A, Roy RP, Sarkar DP (2005). Histidylated lipid-modified Sendai viral envelopes mediate enhanced membrane fusion and potentiate targeted gene delivery. J Biol Chem 280, 35399–35409.

Vester D, Rapp E, Gade D, Genzel Y, Reichl U (2009). Quantitative analysis of cellular proteome alterations in human influenza A virus-infected mammalian cell lines. Proteomics 9, 3316–3327.

Wang X, Sarkar DP, Mani P, Steer CJ, Chen Y, Guha C, Chandrasekhar V, Chaudhuri A, Roy-Chowdhury N, Kren BT, et al. (2009). Long-term reduction of jaundice in Gunn rats by nonviral liver-targeted delivery of Sleeping Beauty transposon. Hepatology 50, 815–824.

Wurth MA, Schowalter RM, Smith EC, Moncman CL, Dutch RE, McCann RO (2010). The actin cytoskeleton inhibits pore expansion during PIV5 fusion protein-promoted cell-cell fusion. Virology 404, 117–126.

Xiao S, Wang Q, Jia J, Cong P, Mo D, Yu X, Qin L, Li A, Niu Y, Zhu K, et al. (2010). Proteome changes of lungs artificially infected with H-PRRSV and N-PRRSV by two-dimensional fluorescence difference gel electrophoresis. Virol J 7, 107.